ChemComm

COMMUNICATION

View Article Online
View Journal | View Issue

Cite this: *Chem. Commun.*, 2025, **61**, 18440

Received 9th September 2025,
Accepted 15th October 2025

DOI: 10.1039/d5cc05205j

rsc.li/chemcomm

The flexible behaviour of a trigonal arylimido iron complex

Andres Gonzalez,[a] Alessandra Casnati,[a] Moritz Willingshofer,[a] Aleksa Radovic,[b] George E. Cutsail III,[bc] Serhiy Demeshko,[d] Franc Meyer[d] and C. Gunnar Werncke*[ae]

A trigonal arylimido iron complex is reported, which is found in an intermediate spin state. The iron bound imido unit is electronically flexible and acts as a nucleophile, reductant, or H atom abstractor. The latter is used for catalytic intramolecular C–H bond amination.

The 3d-metal catalysed amination of (un)-functionalized C–H bonds *via* formal nitrene insertion is an atom economical and environmentally benign approach to secondary amines and thus, has been put under intense scrutiny in recent years.[1,2] It is generally accepted that these amination reactions proceed through highly reactive imido metal intermediates. Though the imido ligand is commonly viewed as a dianionic imide NR^{2-}, for late 3d-metal complexes the metal imido bond becomes more covalent and can also be regarded as either a metal bound imidyl $[NR]^{\bullet -}$ or nitrene $[NR]^{0}$.[3,4] This rationalizes their H atom abstraction (HAA) and/or nitrene transfer capabilities. Authenticated, isolable examples of 3d-metal bound imidyls[5–8] and especially nitrenes[9] are still scarce due to their intrinsic high reactivity.[10] As such, the factors that contribute to their C–H activation reactivity are not fully understood. Furthermore, the 3d-metal bound imido can also react as a dianionic imide,[3] which was, for example, used for catalytic guanylation of carbodiimides.[11,12]

Recently, we reported on the anionic trigonal high-spin iron(II) imidyl complex $[Fe(NMes)X_2]^-$ ($\mathbf{A}^-$, X = N(Dipp)-$SiMe_3$).[7] It exhibited marginal H atom abstraction capabilities due to the sterically encumbered ancillary silylamide ligands. Concurrently, the use of the smaller $-NR_2$ (R = $SiMe_3$) ligand set gave for cobalt an alkyl imide (K{crypt.222}[Co(N^tBu)$(NR_2)_2$]) that was capable of cleaving strong C–H bonds.[13]

With this in mind, the linear iron(I) complex K{crypt}-$[Fe(NR_2)_2]$[14] ([$\mathbf{Fe^I}$]) was reacted with $MesN_3$ (Mes = 2,4,6-trimethylphenyl) at −30 °C in Et_2O. This led to instant gas evolution and rapid precipitation of K{crypt}[Fe(NMes)$(NR_2)_2$], **1**, as a dark green microcrystalline solid (64% yield, Scheme 1, left). X-ray diffraction analysis of **1** (Scheme 1, right) shows most notably an Fe1–N3 bond length of 1.753(2) Å and an Fe1–N3–C_{Aryl} bond angle of 173.04(1)°. The Fe–N_{imido} bond is longer than those found for other imido iron complexes in lower spin states (1.65–1.70 Å).[15,16] It aligns better with those in higher spin states (approx. 1.75 Å),[6–8,12,17–19] for which an imidyl character is mostly discussed.[7,8,17,19] Solid state magnetometry using SQUID gave at ambient temperatures a $\chi_M T$ value of 2.27 $cm^3\ mol^{-1}$ K (μ_{eff} = 4.26μ_B) (Fig. 1A and B), corresponding to a S = 3/2 system. ^{57}Fe Mössbauer spectroscopic analysis at 80 K yielded for **1** an isomer shift δ = 0.36 mm s^{-1} and a quadrupole splitting $|\Delta E_Q|$ = 0.63 mm s^{-1} (Fig. 1C). These features are significantly different to those of the isostructural high-spin (S = 5/2) imido iron complex $\mathbf{A}^-$ (δ = 0.43 mm s^{-1}, $|\Delta E_Q|$ = 4.18 mm s^{-1}),[7] which we attribute to the higher basicity of the used $N(SiMe_3)_2$ ligand. X-band EPR measurement of **1** in THF with 4.5% Bu_4NPF_6 gave the sharpest, most resolved spectrum (Fig. S38) with signals at $g_{eff} \approx 6.7$ and 4.3, indicating reduced aggregation/disorder. The g_{eff} = 6.7 feature showed no

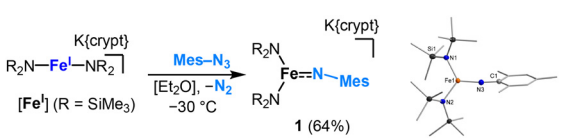

Scheme 1 Left: Synthesis of K{crypt}[Fe(NMes)$(NR_2)_2$], **1**. Right: Molecular structure of the complex anion of **1** (ellipsoids shown at a 50% probability). H atoms are omitted for clarity. Important bond lengths (Å) and angles (°): Fe1–N1 1.945(2), Fe1–N2 1.963(2), Fe1–N3 1.753(2), N3–C_{Aryl} 1.337(2), N1–Fe1–N2 118.08(4), Fe1–N3–C_{Aryl} 173.04(1).

[a] *Department of Chemistry, Philipps-University Marburg, Hans-Meerwein-Straße 4, D-35032 Marburg, Germany. E-mail: gunnar.werncke@chemie.uni-marburg.de, gunnar.werncke@uni-leipzig.de*
[b] *MPI for Chemical Energy Conversion, Stiftstr. 34 – 36, D-45470 Mülheim a. d. Ruhr, Germany*
[c] *Faculty Chemistry and Pharmacy, Ludwig-Maximilians-University Munich, Butenandtstr. 5-13, D-81377 Munich, Germany*
[d] *Institute of Inorganic Chemistry, University of Göttingen, Tammannstr. 4, D-37077 Göttingen, Germany*
[e] *Institute of Chemistry and Crystallography, Faculty of Chemistry, Leipzig University, Johannisallee 29, D-04103, Leipzig, Germany*

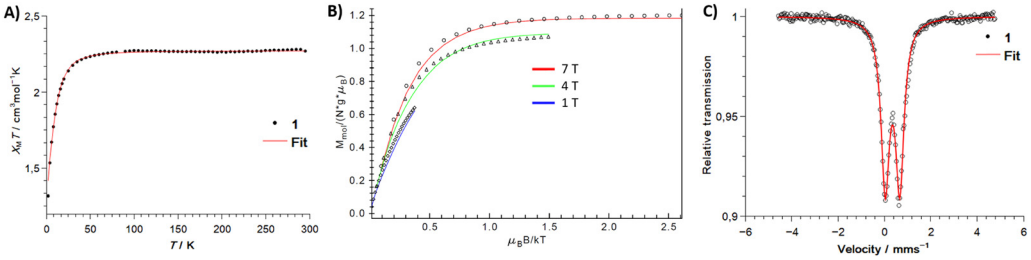

Fig. 1 Plots of $\chi_M T$ *vs.* temperature (A) and variable temperature–variable field magnetization measurements (B) for **1**. The solid line represents the global fit for $S = 3/2$, $g_x = g_y = g_z = 2.20$, $D = 12.1$ cm^{-1} and $E/D = 0$ (fixed). ^{57}Fe Mössbauer spectrum of solid **1** at 80 K ($\delta = 0.36$ mm s^{-1}, $|\Delta E_Q| = 0.63$ mm s^{-1}) (C).

microwave saturation, unlike the $g = 4.3$ signal (Fig. S40), confirming distinct spin species of $S = 3/2$ and 5/2, respectively. The $g = 4.3$ signal is most likely due to sample decomposition, and resembles commonly observed disordered ferric sites.[20] Similar $g_{\text{eff}} \approx 6.1$–$6.3$ signals are reported for three-coordinate $S = 3/2$ Fe$^{\text{III}}$ imido complexes,[16,21] though previously observed higher-field features at $g_{\text{eff}} \approx 1.9$ and 1.5 are absent for **1**, likely due to broadening. Similar features were observed in the spectrum of a solid sample of **1** (Fig. S41). Simulations with two spin components reproduce both frozen solution (THF with 4.5% Bu_4NPF_6) and solid-state data (Fig. S38 and S41), supporting the presence of an $S = 3/2$ species, consistent with the results of the magnetic susceptibility measurements (see SI for more discussion).

For additional insights, the electronic structure of the anion of **1** (coined **1**$^-$) was analysed by the DFT and CASSCF/NEVPT2 methods. DFT calculations gave a quartet (PBE,[22] TPSSh[23]) or a sextet (PBE0[24]) as the ground state. However, only the sextet state geometries align with the experimental solid-state structures (see SI). The computed ^{57}Fe Mössbauer parameters of the solid-state geometry confirmed a quartet state ($\delta_{\text{calc}} = 0.37$ mm s^{-1}, $|\Delta E_{\text{Qcalc}}| = 0.85$ mm s^{-1}), while the sextet state exhibited a drastically larger quadrupole splitting ($\delta_{\text{calc}} = 0.41$ mm, $|\Delta E_{\text{Qcalc}}| = 4.31$ mm s^{-1}) as observed for **A**$^-$. Further calculations using the complete active space self-consistent field (CASSCF,[25] CAS(13,10)) method (PBE0 geometry of the sextet state of **1**$^-$) gave virtually isoenergetic sextet and quartet ground states by *n*-electron valence state perturbation theory (NEVPT2[26]) ($\Delta E_{\text{sext}\rightarrow\text{quar}} = +0.09$ eV). The sextet is represented by a single configuration ($c = 0.9$, Fig. 2, left). The Fe–N π-interaction consists of an iron (Fe : N 0.8 : 0.2) and a nitrogen centred (Fe : N 0.3 : 0.7) bonding orbital, which are paired with the singly occupied anti-bonding combination (Fe : N 0.3 : 0.7 and Fe : N 0.9 : 0.1). Hence, the sextet state is described best as an Fe$^{\text{II}}$ imidyl. Interestingly, the N-centred, singly occupied orbital is orthogonal to the π-system of the aromatic substituent. It is opposed to other aromatic imidyl complexes,[6,19] for which electronic stabilisation by transfer of unpaired spin density onto the aromatic ring is discussed. In the dominant quartet state configuration ($c = 0.60$, Fig. 2, right), the out-of-plane Fe–N π interaction is weak with a doubly occupied nitrogen (π) and a singly occupied iron (π*) centred orbital. In contrast, the in-plane π-interactions are more covalent (Fe : N 0.55 : 0.45; π*: Fe : N 0.4 : 0.6). The two other relevant

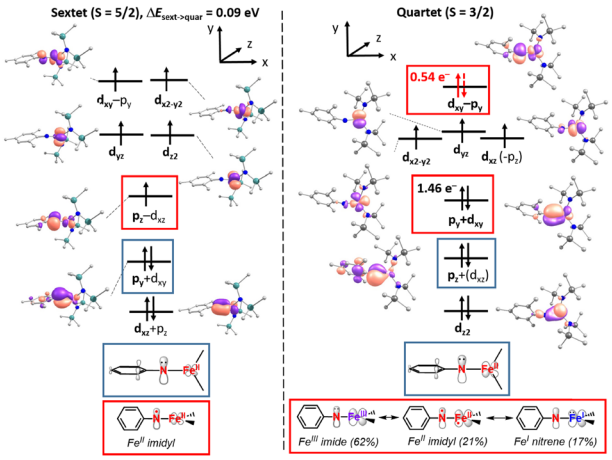

Fig. 2 Electronic structure of **1**$^-$ from CASSCF(13,10)/NEVPT2 calculations with schematic description of the metal/imido interaction. Hydrogen atoms, the aromatic HOMO/LUMO pair and the σ-interaction of the imido ligand are omitted for clarity.

configurations ($c = 0.21$, 0.17) relate to the $\pi\rightarrow\pi^*$ transition within this covalent π/π^* manifold, and leads to population of the LUMO by 0.54 e$^-$. As such the quartet state of **1**$^-$ corresponds to an Fe$^{\text{III}}$ imide with substantial Fe$^{\text{II}}$ imidyl and Fe$^{\text{I}}$ nitrene character.

The ambiguous electronic structure of **1** led us to examine its reactivity. Reaction of two equivalents of MesNCO with **1** resulted in K{crypt}[Fe({OC{NMes}}$_2$NMes}(NR$_2$)$_2$], **2**, (66% yield, Scheme 2). The molecular structure of the anion of **2** contains a six-membered metalla(III) heterocycle. It likely results from two subsequent [2+2] cycloadditions of MesNC═O to a nucleophilic [FeNR] unit in **1**, leading overall to Fe–N bond rupture. The complete bond cleavage of a late 3d-metal imido complex is an unusual feature, observed only for insertion of carbodiimides into the Fe–N bond of an anionic iron(II) imide[12] and of CS_2 into the Fe–N bond of **A**$^-$.[7] **1** shows no nitrene transfer capabilities towards phosphines and alkenes. To probe N-functionalisation by oxidation, **1** was reacted with S_8. It gave the dinuclear iron chalcogenide (K{crypt})$_2$[{Fe(NR$_2$)$_2$}$_2$(μ-S$_3$)(μ-S)], **3** (51% yield), featuring the unusual combination of a bridging sulfide and a rare trisulfide ligand.[27] The fate of the [NR] unit, *e.g.* homo-coupling to a diazene, remained unresolved. The formation of **3** shows that **1** can act as a reductant under electron transfer to S_8. The reaction of the starting [**Fe$^{\text{I}}$**] itself with S_8 was

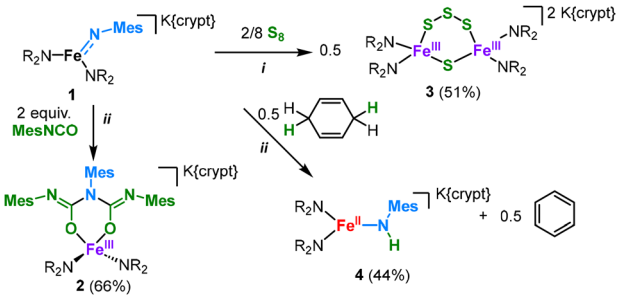

Scheme 2 Synthesis of compounds **2–4** from the reaction of **1** with MesNCO, S_8 or 1,4-cyclohexadiene. (i) 1,2-Difluorobenzene, r.t. (ii) THF/Et_2O, r.t.

previously probed but gave only bis-μ-sulfido bridged species.[28] The selective formation of **3** from an imido metal complex thus represents an unconventional approach to metal chalcogenide clusters. **1** is capable of HAA from 1,4-cyclohexadiene, to give the amide K{crypt}[Fe(N{H}Mes)$(NR_2)_2$], **4**, within 2 h. ^{57}Fe Mössbauer spectroscopic examination gave δ = 0.55 mm s^{-1} and $|\Delta E_Q|$ = 0.88 mm s^{-1}. Interestingly, ^{57}Fe Mössbauer spectroscopic examinations of **1** showed within a day at room temperature formation of a species whose signature matches that of **4** (see SI), hence possible HAA even under solid state conditions.

As such, we examined the linear iron(I) starting complex [**Fe^{I}**] as a precatalyst for the intramolecular C–H bond amination of organoazides. These transformations have been under intense scrutiny since the seminal report on iron from Betley using aliphatic azides,[2,29] which required Boc-protection of the formed N-heterocycle. The respective additive-free catalytic conversions have only been known since recently.[30–32] Reaction of the aromatic azide 1-azido-2-(2-phenylethyl)benzene, **B1**, with 10 mol% [**Fe^{I}**] at 80 °C gave 63% of 2-phenylindoline, **C1** (Scheme 3). Lowering the reaction temperature to 25 °C gave lower yields (42%) and required longer reaction times (18 h). In both cases, the employed azide is fully consumed and points to parallel/subsequent reaction pathways, such as product dehydrogenation. Similar observations were made for related iron-catalysed amination reactions.[30–32] Furthermore, free amine is sometimes observed, which likely stems from stepwise H atom abstraction from the solvent, as observed for the related cobalt complex K{crypt}[Co$(NR_2)_2$].[13] Using the larger K{crypt}[FeX_2]$^-$ resulted for this and all other cases in lower yields. Reaction of 1-azido-2-(3-phenylpropyl)benzene, **B2**, gave 34% of 1,2,3,4-tetrahydro-3-phenylquinoline, **C2**. No turnover was observed for aromatic azides without benzylic sp^3-C–H positions, although initial reaction of [**Fe^{I}**] with the azides gave similar coloured solutions as for **1** that suggest imido formation. Reports of iron-mediated C–H bond amination by aromatic azides are still scarce. In the few known instances[33,34] the reaction was performed at low catalyst loadings but under harsh conditions (*e.g.* 2.5 mol% *N*Bu$_4$[Fe(CO)$_3$NO], 120 °C, microwave 250 W),[33] and with little insights into the involved imido iron species. The aliphatic azide (4-azido-4-methylpentyl)-benzene, **B3**, gave 76% of the amination product 2,2-dimethyl-5-phenylpyrrolidine, **C3**, after 18 h at room temperature. For (5-azido-5-methylhexyl)-benzene, **B4**, the corresponding

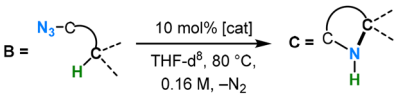

Educt	Product	t /h	[Fe]$^-$	Conv. **B**[a]	Yield **C**[a]
B1	C1	1	[**Fe^{I}**]	>99%	63%
			[FeX_2]$^-$	>99%	58%
B2	C2	18	[**Fe^{I}**]	57%[b]	34%[b]
			[FeX_2]$^-$	65%	29%
B3	C3	18	[**Fe^{I}**]	90%[c]	76%[c]
			[FeX_2]$^-$	70%	68%
B4	C4	18	[**Fe^{I}**]	66%	48% (+17% C4′)[d]
			[FeX_2]$^-$	5%	traces
B5	C5	18[e]	[**Fe^{I}**]	78%	58% (+18% DH[f])
			[FeX_2]$^-$	73%	28% (+16% DH[f])
B6	C6	18	[**Fe^{I}**]	>99%	48%
			[FeX_2]$^-$	>99%	56%

Scheme 3 Iron(I)-mediated catalytic intramolecular C–H amination. [a]Yield by ^{1}H NMR spectroscopy using 1,3,5-trimethoxybenzene as internal standard. [b]After 1 h for [**Fe^{I}**]: conversion = 53%, yield = 29%; [c]room temperature; [d]C4′ = 2,2-dimethyl-6-phenylpiperidine [e]50 °C; [f]DH = dehydrogenated product.

pyrrolidine, **C4**, is obtained in moderate yields (48%, 80 °C) with 17% of the piperidine derivative. Cyclisation is also observed for 1-(1-azido-1-methylethyl)-2-methylbenzene, **B5**, involving a benzylic CH_3 unit (58%). Here, additional dehydrogenation to 1,1-dimethyl-1*H*-isoindole was observed (18%). Finally, (2-azido-2-methylpropyl)benzene (**B6**) was tested with the goal of activating a C(sp^2)–H bond. However, formation of the amine **C6** in 48% yield was observed. This is likely the result of two HAAs from the solvent by the *in situ* formed imido iron(III) complex [Fe(NR′)$(NR_2)_2$]$^-$ as well as by the resulting iron(II) amido complex [Fe(NHR′)$(NR_2)_2$]$^-$. It is instructive to compare the behaviour of [**Fe^{I}**] to that of the divalent Fe$(NR_2)_2$ ([**Fe^{II}**]). The conversion of **B3** to **C3** by [**Fe^{II}**] was reported to require only 1 mol%, but elevated temperatures (120 °C, 24 h, 83%). Here, it was presumed that the reaction is limited by the initial formation of the highly reactive imido iron species due to the reversible formation of the iron organoazide adduct.[35] Contrastingly, for [**Fe^{I}**], the reaction with the azide and the imido formation seems near instantaneous, implying that the HAA or the C–N bond formation is the turn-over limiting step.

In conclusion, we presented the isolation of a trigonal iron aryl imido complex, which is found in an intermediate spin state (S = 3/2) using ^{57}Fe Mössbauer and X-band EPR spectroscopy as well as magnetic measurements. Computational analysis at the CASSCF/NEVPT2 level gave for the quartet state a shared iron(III) imide, imidyl and nitrene character of the imido iron unit. The electronic ambiguity is reflected by the metal bound imido's nucleophilicity, its reduction of S_8 to form an unusual iron sulfide cluster as well as H atom abstraction. The latter ability is exploited

for iron(I) mediated catalytic intramolecular C–H amination using aliphatic and aromatic azides.

Conflicts of interest

There are no conflicts to declare.

Data availability

The data supporting this article are included in the supplementary information (SI). Supplementary information: experimental, analytical, crystallographic and computational details, and further spectra. See DOI: https://doi.org/10.1039/d5cc05205j.

CCDC 2421691–2421694 contain the supplementary crystallographic data for this paper.[36a–d]

Notes and references

1 (*a*) P. Müller and C. Fruit, *Chem. Rev.*, 2003, **103**, 2905–2920; (*b*) Y. Park, Y. Kim and S. Chang, *Chem. Rev.*, 2017, **117**, 9247–9301; (*c*) Y. Liu, T. You, H.-X. Wang, Z. Tang, C.-Y. Zhou and C.-M. Che, *Chem. Soc. Rev.*, 2020, **49**, 5310–5358; (*d*) F. Collet, R. H. Dodd and P. Dauban, *Chem. Commun.*, 2009, 5061–5074; (*e*) D. N. Zalatan and J. Du Bois, in *C–H activation*, ed. J.-Q. Yu and L. Ackermann, Springer, Berlin, 2010, vol. 292, pp. 347–378.
2 D. Bhavyesh, S. Soliya, R. Konakanchi, E. Begari, K. C. Ashalu and T. Naveen, *Chem. – Asian J.*, 2024, **19**, e202301056.
3 A. Grünwald, S. S. Anjana and D. Munz, *Eur. J. Inorg. Chem.*, 2021, 4147–4166.
4 P. F. Kuijpers, J. I. van der Vlugt, S. Schneider and B. de Bruin, *Chem. – Eur. J.*, 2017, **23**, 13819–13829.
5 (*a*) Y. Dong, C. J. Lund, G. J. Porter, R. M. Clarke, S.-L. Zheng, T. R. Cundari and T. A. Betley, *J. Am. Chem. Soc.*, 2021, **143**, 817–829; (*b*) Y. Dong, J. T. Lukens, R. M. Clarke, S.-L. Zheng, K. M. Lancaster and T. A. Betley, *Chem. Sci.*, 2020, **11**, 1260–1268; (*c*) A. Reckziegel, M. Kour, B. Battistella, S. Mebs, K. Beuthert, R. Berger and C. G. Werncke, *Angew. Chem., Int. Ed.*, 2021, **60**, 15376–15380; (*d*) Y. Park, S. P. Semproni, H. Zhong and P. J. Chirik, *Angew. Chem., Int. Ed.*, 2021, **60**, 14376–14380; (*e*) W. Mao, D. Fehn, F. W. Heinemann, A. Scheurer, D. Munz and K. Meyer, *Angew. Chem., Int. Ed.*, 2021, **60**, 16480–16486; (*f*) J. Xiong, Q. Liu, B. Lavina, M. Y. Hu, J. Zhao, E. E. Alp, L. Deng, S. Ye and Y. Guo, *Chem. Sci.*, 2023, **14**, 2808–2820; (*g*) Q. Liu, L. Long, P. Ma, Y. Ma, X. Leng, J. Xiao, H. Chen and L. Deng, *Cell Rep.*, 2021, **2**, 100454; (*h*) J. Cheng, J. Liu, X. Leng, T. Lohmiller, A. Schnegg, E. Bill, S. Ye and L. Deng, *Inorg. Chem.*, 2019, **58**, 7634–7644.
6 M. J. T. Wilding, D. A. Iovan, A. T. Wrobel, J. T. Lukens, S. N. MacMillan, K. M. Lancaster and T. A. Betley, *J. Am. Chem. Soc.*, 2017, **139**, 14757–14766.
7 S. Reith, S. Demeshko, B. Battistella, A. Reckziegel, C. Schneider, A. Stoy, C. Lichtenberg, F. Meyer, D. Munz and C. G. Werncke, *Chem. Sci.*, 2022, **13**, 7907–7913.
8 E. R. King, E. T. Hennessy and T. A. Betley, *J. Am. Chem. Soc.*, 2011, **133**, 4917–4923.
9 (*a*) W. Mao, Z. Zhang, D. Fehn, S. A. V. Jannuzzi, F. W. Heinemann, A. Scheurer, M. van Gastel, S. DeBeer, D. Munz and K. Meyer, *J. Am. Chem. Soc.*, 2023, **145**, 13650–13662; (*b*) K. M. Carsch, I. M. DiMucci, D. A. Iovan, A. Li, S.-L. Zheng, C. J. Titus, S. J. Lee, K. D. Irwin, D. Nordlund, K. M. Lancaster and T. A. Betley, *Science*, 2019, **365**, 1138–1143.
10 C. G. Werncke, *Dalton Trans.*, 2025, **54**, 8374–8384.
11 Y. Gao, M. Pink, V. Carta and J. M. Smith, *J. Am. Chem. Soc.*, 2022, **144**, 17165–17172.
12 Y. Gao, V. Carta, M. Pink and J. M. Smith, *J. Am. Chem. Soc.*, 2021, **143**, 5324–5329.
13 A. Reckziegel, C. Pietzonka, F. Kraus and C. G. Werncke, *Angew. Chem., Int. Ed.*, 2020, **59**, 8527–8531.
14 C. G. Werncke, P. C. Bunting, C. Duhayon, J. R. Long, S. Bontemps and S. Sabo-Etienne, *Angew. Chem., Int. Ed.*, 2015, **54**, 245–248.
15 (*a*) C. M. Thomas, N. P. Mankad and J. C. Peters, *J. Am. Chem. Soc.*, 2006, **128**, 4956–4957; (*b*) S. D. Brown and J. C. Peters, *J. Am. Chem. Soc.*, 2005, **127**, 1913–1923; (*c*) I. Nieto, F. Ding, R. P. Bontchev, H. Wang and J. M. Smith, *J. Am. Chem. Soc.*, 2008, **130**, 2716–2717; (*d*) A. K. Verma, T. N. Nazif, C. Achim and S. C. Lee, *J. Am. Chem. Soc.*, 2000, **122**, 11013–11014; (*e*) S. D. Brown, T. A. Betley and J. C. Peters, *J. Am. Chem. Soc.*, 2003, **125**, 322–323; (*f*) S. C. Bart, E. Lobkovsky, E. Bill and P. J. Chirik, *J. Am. Chem. Soc.*, 2006, **128**, 5302–5303; (*g*) C. Ni, J. C. Fettinger, G. J. Long, M. Brynda and P. P. Power, *Chem. Commun.*, 2008, 6045; (*h*) J. J. Scepaniak, J. A. Young, R. P. Bontchev and J. M. Smith, *Angew. Chem., Int. Ed.*, 2009, **48**, 3158–3160; (*i*) H. Zhang, Z. Ouyang, Y. Liu, Q. Zhang, L. Wang and L. Deng, *Angew. Chem., Int. Ed.*, 2014, **53**, 8432–8436; (*j*) S. Kuppuswamy, T. M. Powers, B. M. Johnson, M. W. Bezpalko, C. K. Brozek, B. M. Foxman, L. A. Berben and C. M. Thomas, *Inorg. Chem.*, 2013, **52**, 4802–4811; (*k*) B. P. Jacobs, P. T. Wolczanski, Q. Jiang, T. R. Cundari and S. N. MacMillan, *J. Am. Chem. Soc.*, 2017, **139**, 12145–12148; (*l*) L. Wang, L. Hu, H. Zhang, H. Chen and L. Deng, *J. Am. Chem. Soc.*, 2015, **137**, 14196–14207.
16 R. E. Cowley, N. J. DeYonker, N. A. Eckert, T. R. Cundari, S. DeBeer, E. Bill, X. Ottenwaelder, C. Flaschenriem and P. L. Holland, *Inorg. Chem.*, 2010, **49**, 6172–6187.
17 M. J. T. Wilding, D. A. Iovan and T. A. Betley, *J. Am. Chem. Soc.*, 2017, **139**, 12043–12049.
18 A. Sridharan, A. C. Brown and D. L. M. Suess, *Angew. Chem., Int. Ed.*, 2021, **60**, 12802–12806.
19 P.-C. Yang, K.-P. Yu, C.-T. Hsieh, J. Zou, C.-T. Fang, H.-K. Liu, C.-W. Pao, L. Deng, M.-J. Cheng and C.-Y. Lin, *Chem. Sci.*, 2022, **13**, 9637–9643.
20 (*a*) E. I. Solomon, T. C. Brunold, M. I. Davis, J. N. Kemsley, S. K. Lee, N. Lehnert, F. Neese, A. J. Skulan, Y. S. Yang and J. Zhou, *Chem. Rev.*, 2000, **100**, 235–350; (*b*) F. Bou-Abdallah and N. D. Chasteen, *J. Biol. Inorg. Chem.*, 2008, **13**, 15–24.
21 N. A. Eckert, S. Vaddadi, S. Stoian, R. J. Lachicotte, T. R. Cundari and P. L. Holland, *Angew. Chem., Int. Ed.*, 2006, **45**, 6868–6871.
22 J. P. Perdew, M. Ernzerhof and K. Burke, *J. Chem. Phys.*, 1996, **105**, 9982–9985.
23 J. Tao, J. P. Perdew, V. N. Staroverov and G. E. Scuseria, *Phys. Rev. Lett.*, 2003, **91**, 146401.
24 C. Adamo and V. Barone, *J. Chem. Phys.*, 1999, **110**, 6158–6170.
25 B. O. Roos, P. R. Taylor and P. E. Sigbahn, *Chem. Phys.*, 1980, **48**, 157–173.
26 C. Angeli, R. Cimiraglia, S. Evangelisti, T. Leininger and J.-P. Malrieu, *J. Chem. Phys.*, 2001, **114**, 10252–10264.
27 A. Aruffo, E. C. Lingafelter, B. D. Santarsiero and V. Schomaker, *Acta Crystallogr., Sect. A: Found. Crystallogr.*, 1981, **37**, C218–C218.
28 C. Schneider, S. J. Groß, S. Demeshko, S. Bontemps, F. Meyer and C. G. Werncke, *Chem. Commun.*, 2021, **57**, 10751–10754.
29 (*a*) E. T. Hennessy and T. A. Betley, *Science*, 2013, **340**, 591–595; (*b*) B. Bagh, D. L. J. Broere, V. Sinha, P. F. Kuijpers, N. P. van Leest, B. de Bruin, S. Demeshko, M. A. Siegler and J. I. van der Vlugt, *J. Am. Chem. Soc.*, 2017, **139**, 5117–5124.
30 W. Stroek, M. Keilwerth, D. M. Pividori, K. Meyer and M. Albrecht, *J. Am. Chem. Soc.*, 2021, **143**, 20157–20165.
31 W. Stroek, L. Hoareau and M. Albrecht, *Catal. Sci. Technol.*, 2023, **13**, 958–962.
32 W. Stroek and M. Albrecht, *Chem. Sci.*, 2023, **14**, 2849–2859.
33 I. T. Alt, C. Guttroff and B. Plietker, *Angew. Chem., Int. Ed.*, 2017, **56**, 10582–10586.
34 (*a*) S. K. Das, S. Das, S. Ghosh, S. Roy, M. Pareek, B. Roy, R. B. Sunoj and B. Chattopadhyay, *Chem. Sci.*, 2022, **13**, 11817–11828; (*b*) I. T. Alt and B. Plietker, *Angew. Chem., Int. Ed.*, 2016, **55**, 1519–1522.
35 (*a*) W. Stroek, M. Keilwerth, L. A. Malaspina, S. Grabowsky, K. Meyer and M. Albrecht, *Chem. – Eur. J.*, 2024, **30**, e202303410; (*b*) A. Gonzalez, S. Demeshko, F. Meyer and C. G. Werncke, *Chem. Commun.*, 2023, **59**, 11532–11535.
36 (*a*) CCDC 2421691: Experimental Crystal Structure Determination, 2025, DOI: 10.5517/ccdc.csd.cc2m8z2z; (*b*) CCDC 2421692: Experimental Crystal Structure Determination, 2025, DOI: 10.5517/ccdc.csd.cc2m8z30; (*c*) CCDC 2421693: Experimental Crystal Structure Determination, 2025, DOI: 10.5517/ccdc.csd.cc2m8z41; (*d*) CCDC 2421694: Experimental Crystal Structure Determination, 2025, DOI: 10.5517/ccdc.csd.cc2m8z52.